

# Computational Structural Analysis and Homology Modelling of Beta-Xylanase from *Bifidobacterium pullorum*: A Comprehensive In-Silico Investigation

Abdul Qadeer Baseer\*<sup>1</sup>, Shafiqullah Mushfiq<sup>1</sup>, Abdul Wahid Monib<sup>1,2</sup>, Mohammad Hassan Hassand<sup>1,3</sup> and Parwiz Niazi<sup>1</sup>

<sup>1</sup>Department of Biology, Faculty of Education, Kandahar University, Kandahar, AFGHANISTAN.

<sup>2</sup>School of Environmental Sciences, Jawaharlal Nehru University, New Delhi, INDIA.

<sup>3</sup>Faculty of Biology and biotechnology, Al Farabi Kazakh National University, 71 Al-Farabi Ave, Almaty 050040, KAZAKHSTAN.

\*Corresponding Author: a.baseer@kdru.edu.af



www.jrasb.com || Vol. 2 No. 6 (2023): December Issue

Received: 03-12-2023

Revised: 05-12-2023

Accepted: 07-12-2023

## ABSTRACT

*Bifidobacterium pullorum*, commonly found in chicken waste and preferring mesophilic characteristics, contains an enzyme known as Beta-Xylanase. This enzyme effectively breaks down xylan, offering potential for creating biogas, like methane, and biofuels, such as ethanol. Scientists are actively exploring sustainable energy sources, while industries aim for cost-effective methods to decrease operational expenses. The conventional methods for producing biogas and biofuels involve high-temperature processes using fuel combustion, leading to significant expenses. To address this, mesophilic bacteria present a promising alternative for more cost-efficient biofuel production. This study is the first to delve into the genomic and three-dimensional structure of beta-xylanase, crucial for breaking down xylan. Our findings highlight that the beta-xylanase in *Bifidobacterium pullorum* showcases a TIM-barrel structure, similar to other GH10 xylanases essential in carbohydrate breakdown. This indicates a potential connection between *Bifidobacterium pullorum*'s beta-xylanase and the improvement of biogas production.

**Keywords-** Mesophilic, Beta-xylanase, Biogas, Xylan, Bio-renewable energy, Genomic.

## I. INTRODUCTION

Beta-xylanase (EC 3.2.1.8) represents a glycosidase enzyme crucial in catalysing chemical reactions leading to the degradation of xylan, a polymer characterized by a beta-1,4-linked D-xylose backbone. This enzyme is pivotal in breaking down xylan into xylose and other sugars. Various organisms like bacteria, algae, and fungi are capable of producing xylanases. Xylose, a product of this breakdown, serves as a primary carbon source vital for cell metabolism and significantly influences plant cell susceptibility to infection by pathogens [1].

Xylan constitutes a significant portion of hemicellulose, the second most prevalent polysaccharide

within the cell wall and the central lamella in plant cells, following cellulose. Hemicellulose, a complex polymeric carbohydrate, comprises approximately 30% of plant cell walls and includes diverse polysaccharides like xylan, xyloglucan, glucomannan, galactoglucomannan, and arabinogalactan. Xylanases specifically target xylan, degrading it into its constituent monosaccharides [2, 3]. Since xylan can be broken down into xylose and other sugars, it presents a potential energy source that could be harnessed in the generation of renewable energy. Bio-digesters play a vital role in generating biogas, a process facilitated by multiple anaerobic bacteria that secrete hydrolyzing enzymes to break down lignocellulose. Oyewole (2010) identified various anaerobic bacteria in chicken feces contributing

to biogas production within the mesophilic temperature range of the bio-digester. Consequently, *B. pullorum*, isolated from chicken feces, emerges as a potential producer of hydrolyzing enzymes crucial for biogas production. Its mesophilic nature allows *B. pullorum* to flourish in the bio-digester environment, yielding significant quantities of beta-xylanase capable of degrading the lignocellulose component [4].

Beta-xylanase, an enzyme prevalent in numerous microorganisms like Bacterioides, Clostridia, and Enterobacteriaceae (Weiland, 2010), serves as the focus of this study. The objective is to model its 3D structure and elucidate the functional aspects of this newly discovered enzyme in *Bifidobacterium pullorum*. Additionally, *Bifidobacterium pullorum*, being a mesophilic bacterium, offers an alternative for biogas production compared to thermophilic bacteria, which demand higher energy inputs [5]. Parawira W. (2004) emphasized that biogas production entails biological processes within the bio-digester, converting organic matter such as agricultural or animal waste into a blend of methane and carbon dioxide [6]. Leveraging the mesophilic trait of *Bifidobacterium pullorum* holds promise for potentially reducing the expenses associated with renewable energy production.

## II. METHODOLOGY

### 2.1 Sequence Retrieval Databases

The FASTA-formatted sequence (A0A087CCI8) was sourced from the UniProt database (<https://www.uniprot.org/uniprot/A0A087CCI8>) specifically for conducting structural analysis. As of now, there exists no known structure for this specific enzyme, beta-xylanase from *Bifidobacterium pullorum*. To identify its domain and active site, the target sequence underwent analysis utilizing the online tool ScanProsite (<https://prosite.expasy.org/scanprosite>). This process aimed to delineate the structural and functional elements within the sequence for further investigation.

### 2.2 Multiple Sequence Alignments (MSA)

A multiple sequence alignment (MSA) was carried out using UniProt (<https://www.uniprot.org/>) to compare the target sequence with similar enzymes found in other bacteria and fungi. Specifically, the alignment involved the target sequence and 10 fungi and 10 bacteria, including species such as *Bifidobacterium catenulatum*, *Bifidobacterium reuteri*, *Microbacterium sp.*, *Leifsonia sp.*, *Agromyces sp.*, *Lysinimonas sp.*, *Cellulomonas sp.*, *Jonesia denitrificans*, *Promicromonospora thailandica*, and *Trichoderma pseudokoningii*. Additional species such as *Trichoderma longibrachiatum*, *Trichoderma orientale*, *Hypocrea virens*, *Morchella conica*, *Trichoderma parareesei*, *Hypocrea jecorina*, *Bionectria ochroleuca*, *Trichoderma asperellum*, and *Aspergillus wentii* were included as shown in Table 1."

**Table 1: List of the organisms used for alignment (Bacteria and Fungi)**

UniProt ID	Gene Name	Organism (Bacteria)
A0A087CCI8	BPULL_0537	<i>Bifidobacterium pullorum</i>
A0A087AT52	BKAS_1991	<i>Bifidobacterium catenulatum</i>
A0A087CMF7	BREU_1231	<i>Bifidobacterium reuteri</i>
A0A3G6ZJY2	DT073_04480	<i>Microbacterium sp.</i>
A0A0Q8CIX9	ASD61_16125	<i>Leifsonia sp.</i>
A0A4V0YHI0	ET445_17015	<i>Agromyces sp.</i>
A0A387B3P2	D7147_07955	<i>Lysinimonas sp.</i>
A0A4P7SK83	E5225_14650	<i>Cellulomonas sp.</i>
C7R5M3	Jden_1648	<i>Jonesia denitrificans</i>
A0A397LXM6	C7338_2965	<i>Promicromonospora thailandica</i>
Fungi		
B0FXL9	ex1	<i>Trichoderma pseudokoningii</i>
A0A2T4CGL8	M440DRAFT_1325428	<i>Trichoderma longibrachiatum</i>
A0A0C5LDI6	XYNIII	<i>Trichoderma orientale</i>
G9MUR3	TRIVIDRAFT_53264	<i>Hypocrea virens</i>
A0A3N4L390	P167DRAFT_569824	<i>Morchella conica</i>
A0A2H2ZE97	A9Z42_0059570	<i>Trichoderma parareesei</i>
Q9P973	xyn3	<i>Hypocrea jecorina</i>
A0A0B7KBM5	BN869_000008189_1	<i>Bionectria ochroleuca</i>
A0A2T3YTC8	M441DRAFT_62499	<i>Trichoderma asperellum</i>
A0A1L9RIF0	ASPWEDRAFT_182798	<i>Aspergillus wentii</i>

### 2.3 Primary and Secondary Sequence Analysis

The molecular characteristics of Beta-xylanase derived from *Bifidobacterium pullorum* were deduced through sequence analysis using the ExPASy ProtParam tool (<https://web.expasy.org/protparam/>). Furthermore, predictions regarding the secondary structure of the sequence were made utilizing the CFSSP server (<http://www.biogem.org/tool/chou-fasman/>). This particular server identifies distinct regions encompassing alpha helices, beta sheets, and turns within the sequence.

### 2.4 Three-dimensional (3D) Structure Modelling

Homology modelling of beta-xylanase was executed through the SWISS-MODEL server, accessible at <https://swissmodel.expasy.org/>. This modelling procedure entailed utilizing templates sourced from the Protein Data Bank (PDB), accessible at <https://www.rcsb.org/>. The resulting structure prediction was visualized using PyMol to gain insights into the generated model.

### 2.5. 3D Structure Analysis

#### 2.5.1 Comparison with Template

A superimposition was conducted between the forecasted structure of beta-xylanase generated by SWISS-MODEL and an artificial enzyme for

*Escherichia coli* (6FHF) retrieved from the PDB database. This comparison aimed to assess any resemblances or disparities between the two structures. The examination, analysis, and comparison of the predicted structure with the template were visualized using the PyMol software available at <https://pymol.org/2/>.

### 2.5.2 3D Model Quality

The assessment of the 3D structure quality of beta-xylanase from SWISS-MODEL was conducted using the SAVES v5.0 server, accessible at <https://servicesn.mbi.ucla.edu/SAVES/>. This server encompasses five distinct validation approaches: Procheck, Verify 3D, Errat, Procheck, and Prove. Specifically, for this study, Procheck, Verify 3D, and Errat servers were employed to validate and assess the reliability of the 3D protein structure.

### 2.5.3 Conserve 3D Domain

The PyMol software was utilized to conduct a comparative analysis, emphasizing the distinct domains present within the 3D modelled Beta-xylanase from *Bifidobacterium pullorum* and the template of an artificial enzyme obtained from *Escherichia coli*.

## III. RESULT & DISCUSSION

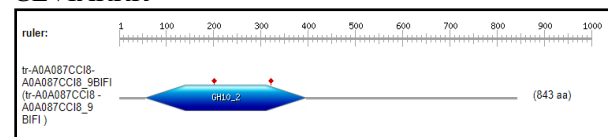
### 3.1 Amino acids Sequence Retrieval

The sequence of Beta-xylanase from *Bifidobacterium Pullorum*, specifically identified as A0A087CCI8, was retrieved from the UniProt database.

**Table 2: The amino acid sequence of Beta-xylanase for *Bifidobacterium pullorum* (UniProt ID: A0A087CCI8)**

```
>tr|A0A087CCI8|A0A087CCI8_9BIFI Beta-xylanase
OS=Bifidobacterium pullorum OX=78448
GN=BPULL_0537 PE=3 SV=1
MDTLFNTTDERGASKRRGIVAALAAAAMLLPLA
FSPTAMAADPDYPGGIKGEYNPLGINAGVAIETY
TLNQDKEKALVENFDQITPENSLKPEGWYDDQH
NFRMSVDARNLLTFASENGIKVYGHVWVWHSQT
PDWFFQADEGCHDNTDNPVTSCLPADKATMQE
RQRRIENVAKAISDEFKFGSPTNPVVAFDVNV
ETVNDGDDPATNGMRNSLWYQTYGGEDIYDA
FRNANTYLNVDVYAADDAEHPVTLFINDYGTEQA
GKRSRYKALVERMIQQGVPFDGIGHQFHVSLTTA
SSNLDDALTDMSLGKKQAITELDVATGTPVTEA
KLIEQGRYYYDVNQIHRHADQLFSVSVWGLSDD
QSWRNKEGAPLLFDENLNRKPAYVGYIGDEDNL
PEPMKSAIVFKDPSATVDSPLPGTEPRNGASSPWE
RLPLITLNASEDGTTVAGTFNAYWVNDGTLNDGTL
NDGTLTVYVDAVDVTKSDGDSVTVRVGDAEYVI
GRSSSPAADVASKVVEGDGGYELVVTVPCPDA
VENAAVGLNVIVKDGDSGQAAAWDTNPTGTVTL
VEPLSYTEAVKVPADVEAPKIDADASDAAWDDA
VEVALDKVTSATPEATATAKTLWSDGKLYVLMET
VTDADIDLNSNPWEKDSVEVYIDRGNTKSGQYT
```

```
DDIQIRVSADGKELSGAGAAEDVQKSRVSTAG
REVDGGYVEMAIIDLGEAAAGTFEGVDFQINDA
KNGARIGIRNWADPTGAGYQTASHWGVLRLLAD
PSETETPGGEDPETPGDEGTPGGDTEKPSDEKPRP
SDDADNDDKMPQTGSAVIGVAVVALLVAAGC
GLVIARRR
```



(a)

Predicted features:			
DOMAIN	57	396	GH10 [condition: none]
ACT_SITE	201		Proton donor [condition: E]
ACT_SITE	321		Nucleophile [condition: E]

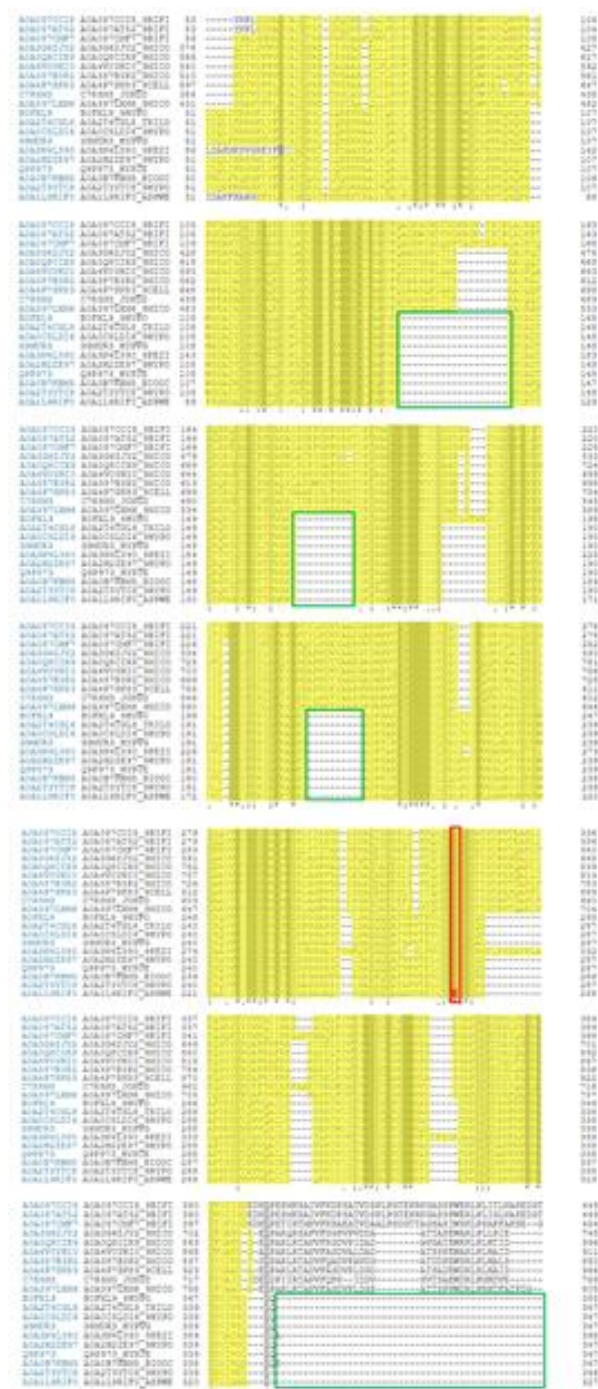
(b)

**Figures 1: (a) According to ScanProsite analysis, the Beta-xylanase found in *Bifidobacterium pullorum* (A0A087CCI8) encompasses a singular domain recognized as a glycosyl hydrolase 10 domain (GH10). This domain extends from amino acid 57 to 396 within the sequence. (b) Furthermore, the analysis indicated the likelihood of two active sites situated at glutamic acid residues 201 and 321 within the GH10 domain. These sites serve distinct roles: residue 201 acts as a proton donor, while residue 321 functions as a nucleophile.**

### 3.2 Multiple sequence alignment Between Bacteria and Fungi

The multiple sequence alignment analysis, depicted in Figure 2, revealed intriguing insights into the comparison of bacterial and fungal species' sequences. Notably, the positions of identity and similarity were found to be 2.786% and 66%, respectively, highlighted in grey. In this comparison of bacteria and fungi sequences, a common glycosyl hydrolase family 10 (GH10) domain, denoted by yellow coloration, was observed. Additionally, while the active site (depicted in red) was specifically illustrated for *Aspergillus wentii*, the shared presence of glutamic acid at this position (highlighted in the red box) across all organisms suggests a conserved active site. This observation aligns with ScanProsite predictions, reaffirming the shared active site among these organisms, substantiating their capability to degrade xylan due to the common catalytic domain. However, an intriguing distinction emerges regarding fungi having a reduced number of amino acids, resulting in the absence of carbohydrate-binding protein or carbohydrate-binding modules (CBM). Previous reports by Teo et al. (2019) suggest that CBM plays a pivotal role in catalytic activities, affinities, and specificity of enzymes [7]. This difference prompts further exploration to determine the implications on the rate of xylan degradation activities in both bacteria and fungi. The comparison in Figure 2, represented by the green box, indicates a shorter amino acid sequence in fungi compared to bacteria, signifying significant differences between these organisms. This divergence likely stems from their

classification into distinct kingdoms, with bacteria belonging to the prokaryotic kingdom and fungi to the eukaryotic kingdom.



Legend: ■ Active site ■ Domain ■ Similarities

Figure 2: The analysis of multiple sequence alignment was conducted for a combination of bacteria and fungi that shared the same Beta-xylanase.

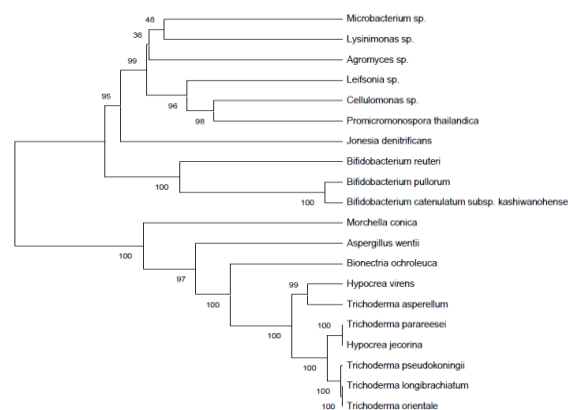
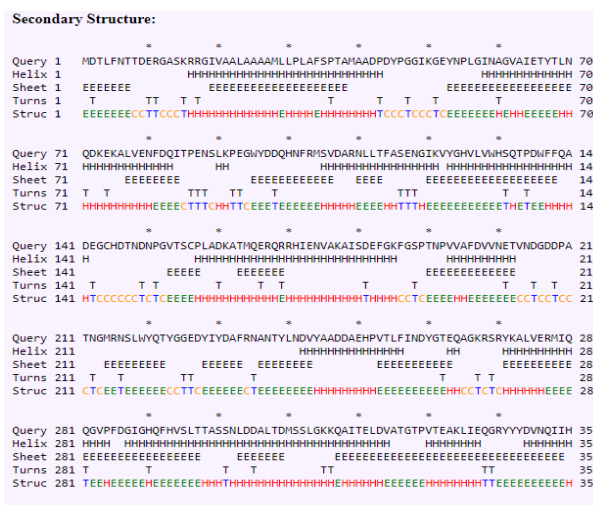
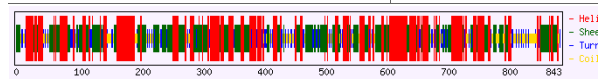


Figure 3: The phylogenetic tree for combination of bacteria and fungi that shared the same Beta-xylanase.

### 3.3 Primary and Secondary Sequence Analysis

Table 3: The molecular properties of Beta-xylanase from *Bifidobacterium Pullorum* obtained from ExPASy ProtParam tool.

Number of amino acids	843
Molecular weight	90494.38
Theoretical pI	4.30
Total number of negatively charged residues (Asp + Glu)	138
Total number of negatively charged residues (Arg + Lys)	66
Formula	C <sub>3954</sub> H <sub>6109</sub> N <sub>1077</sub> O <sub>1328</sub> S <sub>16</sub>
Instability index	The instability index (II) is computed to be 27.99. This classifies the protein as stable.
Aliphatic index	75.47



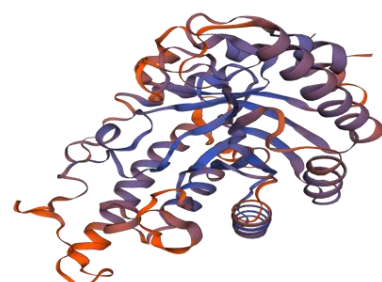


**Figure 4: Result of secondary structure prediction of beta-xylanase of *Bifidobacterium pullorum* from CFSSP.**

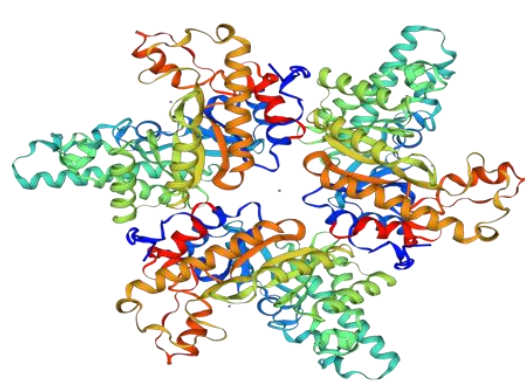
According to the findings from the CFSSP server, as displayed in Figure 4, the analysis of the targeted sequence aimed to predict the secondary structure regions, including alpha helix, beta-sheet, and turns. Among the 842 total residues, the results indicated that 503 residues (59.7%) contributed to the formation of alpha helices, 437 residues (51.8%) contributed to beta-sheet formation, and 128 residues (15.2%) contributed to turn formations within the protein structure.

**3.4 Three-dimensional (3D) Structure Modelling**

The SWISS-MODEL homology modelling was utilized to predict the 3D structure of Beta-xylanase derived from *Bifidobacterium pullorum*. The server generated the predicted structure, represented in Figure 9(a), utilizing 50 available templates for comparative analysis with the model structure prediction. From the array of templates accessible, the artificial enzyme for *Escherichia coli* (6FHF) was selected for the model prediction, as illustrated in Figure 9(b). The predicted structure of Beta-xylanase displayed a 34.38% identity to the selected template.

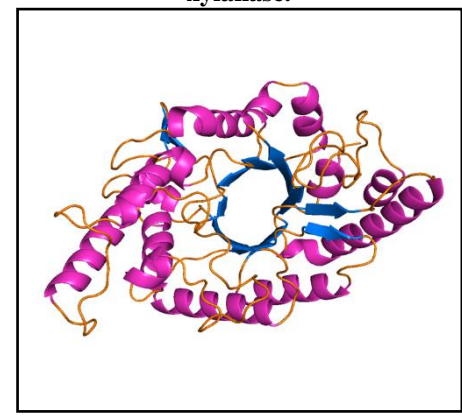


(a)

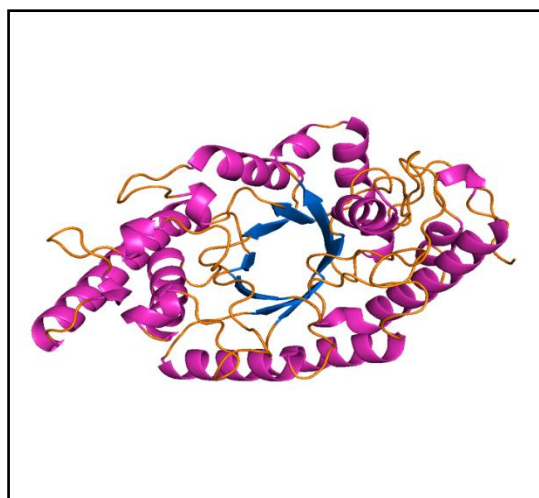


(b)

**Figures 5: (a) The 3D structure of beta-xylanase for *Bifidobacterium pullorum* obtained through Swiss Model homology modelling. (b) The 3D structure of the artificial enzyme for *Escherichia coli* (6FHF) used as a template for the modelling of beta-xylanase.**



(a)



(b)

Figures 6: The 3D structure of the beta-xylanase from *Bifidobacterium pullorum*, generated by Swiss Model, was visualized using PyMol. The structure was coloured based on its secondary structure, and the result is shown in figure (a). The artificial enzyme for *Escherichia coli* (6FHF) was used as a template for the modeling, and its structure was also visualized using PyMol and coloured based on secondary structure as shown in figure (b).

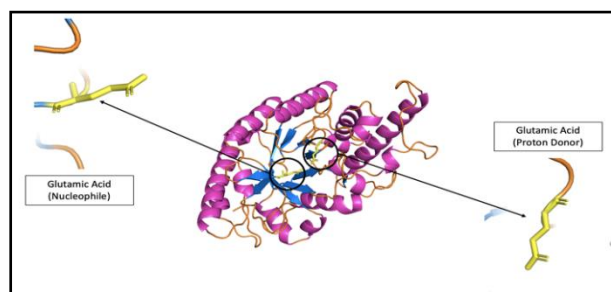


Figure 7: The three-dimensional structure of *Bifidobacterium pullorum*'s beta-xylanase with the active sites

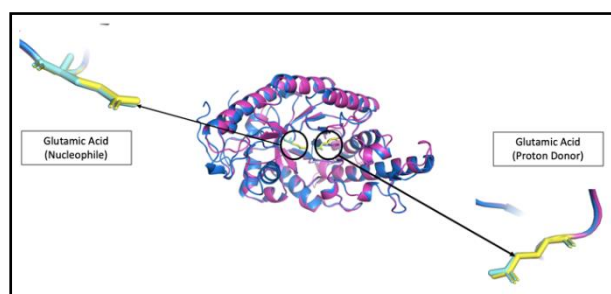


Figure 8: The 3D structure of the beta-xylanase from *E. coli* (in blue) and *B. pullorum* (in magenta) were superimposed with the active sites highlighted. The active sites were marked with cyan color for the template and yellow color for *B. pullorum*.

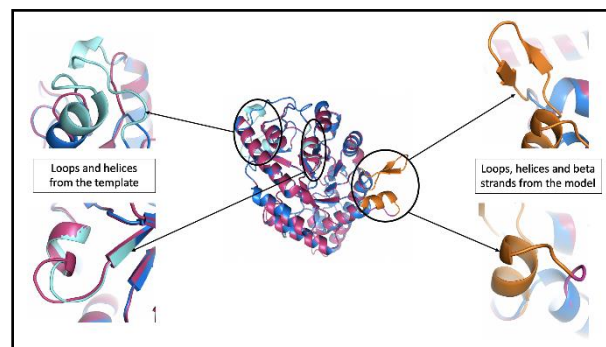


Figure 9: The 3D structures of beta-xylanase from *E. coli* and *B. pullorum* were superimposed, with the template shown in blue and the model in magenta. Differences between the two structures were highlighted, with the template shown in cyan and the *B. pullorum* structure shown in orange.

### 3.5 3D Structure Analysis

#### 3.5.1 Comparison with Template

The 3D structures of beta-xylanase from *E. coli* and *B. pullorum* were modelled via Swiss Model, presented in Figure 5(a) and 5(b), respectively. PyMol facilitated the visualization of both organisms' modelled structures. Figure 6(a) illustrates the secondary structure of *B. pullorum*, portraying beta strands in blue, helices in magenta, and loops/turns in orange.

Both *B. pullorum* and *E. coli* model structures reveal a TIM barrel, a conserved protein fold characterized by eight helices and eight parallel beta strands alternating along the peptide backbone, showcased in Figures 6(a) and 6(b). The TIM barrel incorporates flexible beta-alpha loops responsible for substrate binding and shielding the catalytic site from the surrounding solvent [8]. Studies by Gromiha et al. (2004) revealed stabilizing residues in beta-xylanase located in the N- and C-terminal loops and alpha helices, with the majority situated in the beta-sheets [9]. Additionally, Silverman et al. (2002) proposed the significance of beta-sheet amino acids in maintaining the stability of TIM barrel structures, while amino acids within alpha helices and loops were deemed less critical due to their greater flexibility [10].

The PyMol-enabled superimposition of the modelled 3D structures of beta-xylanase from *B. pullorum* and *E. coli*, depicted in figure 8, unveiled remarkable similarity despite slight differences in sequence length (1185 bp for *B. pullorum* and 1128 bp for *E. coli*). However, nuanced structural disparities emerged, notably the presence of additional orange-coloured loops, beta strands, and helices in *B. pullorum*, contrasted by cyan-coloured loops and helices in *E. coli* (Figure 9).

Despite these structural distinctions, the superimposed 3D models showcased the overlapping of their active sites. Both enzymes exhibited dual active

sites, represented by yellow and cyan sticks in figure 8. In *B. pullorum*, the active site resides at amino acids 201 and 321, featuring glutamic acid functioning as a proton donor and nucleophile. Similarly, in *E. coli*, glutamic acid is pivotal at amino acids 157 and 265. Earlier studies suggested that the catalytic mechanism of GH10 endoxylanase involves two glutamate residues, following a double displacement reaction [11, 12].

GH10 enzymes, to which this enzyme belongs, are generally known for their versatility in hydrolyzing various polysaccharides with differing side chain modifications [13]. For glycosyl hydrolases, two distinct catalytic mechanisms, retaining and inverting, have been proposed to cleave glycosidic bonds, both extensively studied. Retaining and inverting enzymes feature active sites formed by two glutamic acid residues situated approximately 5.5Å and 9.5-7.5Å apart, respectively [14, 15]. In inverting enzymes, the distance between catalytic residues is suggested to be less constrained compared to retaining enzymes. Family 10 xylanase, catalysing hydrolysis through a retaining mechanism, operates via a double displacement reaction [16].

### 3.5.2 Model Quality

The predicted 3D structure underwent validation through various methods, including Verify, Errat, and ProCheck. Verify analysis aimed to gauge the 3D model's compatibility with the amino acid sequence, categorizing structural classes based on the arrangement and environment of alpha helices, beta strands, loops, polar, and nonpolar structures. Results showed that 88.54% of the residues attained an average 3D-1D score of  $\geq 0.2$ , indicating favourable compatibility.

Errat assessment evaluated the overall quality of the model by examining non-bonded interactions among diverse atoms in the protein structure. The model achieved an overall quality factor of 80.304, signifying a high-quality model based on this criterion. Furthermore, ProCheck analysis was employed to appraise the model's quality by comparing its stereochemistry with that observed in high-resolution crystal structures. Remarkably, results demonstrated that 95.2% of the residues fell within the most favored regions of the Ramachandran plot, a strong indication of excellent stereochemical quality (Figure 10).



Figure 10: Structure quality check from Verify 3D.

Also, the utilization of the Errat server involved analysing non-bonded interaction statistics among different atom types and plotting the error function values across a nine-residue sliding window. This detailed analysis unveiled an impressive quality factor of

93.8416% for the predicted structure. Taken collectively, the outcomes derived from these validation tools strongly indicate that the forecasted 3D structure of beta-xylanase originating from *B. pullorum* attains high-quality standards. Consequently, this structure holds significant promise for subsequent analyses and molecular docking studies [16].



Figure 11: Errat Error values for predicted structure of Beta-xylanase of *Bifidobacterium Pullorum*.

On the other hand, ProCheck serves as a tool to scrutinize a protein structure's stereochemical quality by meticulously examining residue-by-residue geometry and generating PostScript plots. The outcomes from ProCheck unveiled a Ramachandran plot showcasing 89.9% of residues in the favoured region, 9.1% in the allowed region, and a mere 1.0% in the outlier region, depicted in figure 12. This distribution highlights an overwhelmingly high percentage of residues occupying the preferred regions within the plot, signifying excellent stereochemical quality and structural reliability.

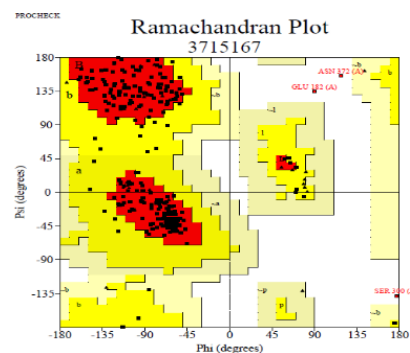


Figure 12: Structure quality check from Ramachandran Plot.

Table 3: Summary of quality check of 3D model from ERRAT, Verify 3D and Procheck servers.

TOOL	FUNCTION	QUALITY	VALUE	ACCEPTED RANGE
Verify 3D	Determine the compatibility of 3D atomic model.	GOOD	88.54%	At least 80% of the amino acids have scored $\geq 0.2$ in the 3D/1D profile.
Errat	Determine protein structures	GOOD	93.84%	$>95\%$

	by crystallograph y.			
Prochec k	Check the protein structure stereochemica l quality.	GOOD	99.0%	>90%

### 3.5.3 Conserve 3D Domain

The enzyme's entire structure is characterized by a single conserved domain known as the glycosyl hydrolase 10 (GH10) domain, distinctly highlighted in red colour within figure 13. This domain represents a fundamental and conserved element throughout the entire enzyme structure.

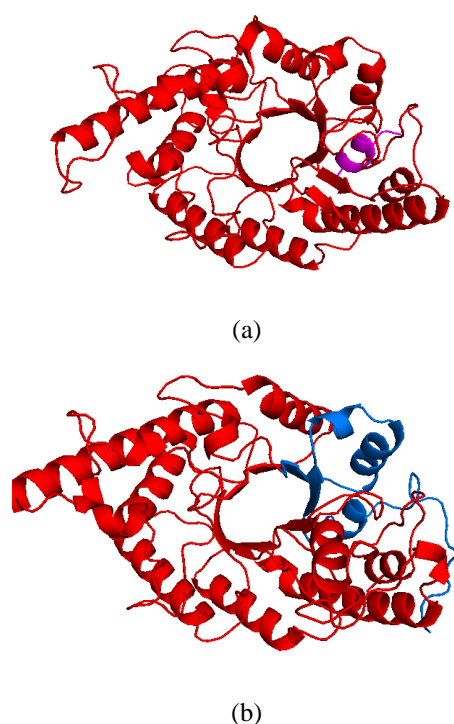


**Figure 13: The 3D structures of Beta-xylanase from *Bifidobacterium Pullorum* (shown in figure a) and the template of an artificial enzyme from *Escherichia coli* (shown in figure b) were visualized using PyMol, with the conserved glycosyl hydrolase 10 domain highlighted in red.**

## IV. CONCLUSION

The enzyme beta-xylanase derived from *Bifidobacterium pullorum* exhibits a TIM-barrel structure similar to the artificial enzyme template of *Escherichia coli* and other GH10 xylanases. The primary function of the glycosyl hydrolase 10 domain (GH10) lies in the degradation of carbohydrates, particularly xylan substrates, leading to the production of xylose. This conversion to xylose bears significant promise, particularly in the realms of renewable energy

production and prospective biotechnological applications. The enzymatic breakdown of xylan into xylose signifies a pivotal avenue for harnessing xylose as a potential renewable energy source and underscores its potential significance in various industrial and biotechnological applications in the future.

## REFERENCES

- [1]. Prade, R. A. (1996). Xylanases: from biology to biotechnology. *Biotechnology and Genetic Engineering Reviews*, 13(1), 101-132.
- [2]. Shekiri, J., Kuhn, E. M., Selig, M. J., Nagle, N. J., Decker, S. R., & Elander, R. T. (2012). Enzymatic conversion of xylan residues from dilute acid-pretreated corn stover. *Applied biochemistry and biotechnology*, 168, 421-433.
- [3]. Polizeli, M. D. L. T. D. M., Rizzatti, A. C. S., Monti, R., Terenzi, H. F., Jorge, J. A., & Amorim, D. D. S. (2005). Xylanases from fungi: properties and industrial applications. *Applied microbiology and biotechnology*, 67, 577-591.
- [4]. Weiland, P. (2010). Biogas production: current state and perspectives. *Applied microbiology and biotechnology*, 85, 849-860.
- [5]. Parawira, W. (2004). Anaerobic Treatment of Agricultural Residues and Wastewater-Application of High-Rate Reactors.
- [6]. Teo, S. C., Liew, K. J., Shamsir, M. S., Chong, C. S., Bruce, N. C., Chan, K. G., & Goh, K. M. (2019). Characterizing a halo-tolerant GH10 xylanase from *Roseithermus sacchariphilus* strain RA and its CBM-truncated variant. *International journal of molecular sciences*, 20(9), 2284.
- [7]. Wierenga, R. K. (2001). The TIM-barrel fold: a versatile framework for efficient enzymes. *FEBS letters*, 492(3), 193-198.
- [8]. Gromiha, M. M., Pujadas, G., Magyar, C., Selvaraj, S., & Simon, I. (2004). Locating the stabilizing residues in ( $\alpha/\beta$ ) 8-barrel proteins based on hydrophobicity, long-range interactions, and sequence conservation. *PROTEINS: Structure, Function, and Bioinformatics*, 55(2), 316-329.
- [9]. Silverman, J. A., & Harbury, P. B. (2002). The equilibrium unfolding pathway of a ( $\beta/\alpha$ ) 8 barrel. *Journal of molecular biology*, 324(5), 1031-1040.
- [10]. Henrissat, B., & Davies, G. (1997). Structural and sequence-based classification of glycoside hydrolases. *Current opinion in structural biology*, 7(5), 637-644.
- [11]. Rye, C. S., & Withers, S. G. (2000). Glycosidase mechanisms. *Current opinion in chemical biology*, 4(5), 573-580.
- [12]. Biely, P., Vršanská, M., Tenkanen, M., & Kluepfel, D. (1997). Endo- $\beta$ -1, 4-xylanase families: differences in catalytic properties. *Journal of biotechnology*, 57(1-3), 151-166.
- [13]. Collins, T., Gerday, C., & Feller, G. (2005).

Xylanases, xylanase families and extremophilic xylanases. *FEMS microbiology reviews*, 29(1), 3-23.

[14]. Skariyachan, S., & Garka, S. (2018). Exploring the binding potential of carbon nanotubes and fullerene towards major drug targets of multidrug resistant bacterial pathogens and their utility as novel therapeutic agents. In *Fullerens, Graphenes and Nanotubes* (pp. 1-29). William Andrew Publishing.

[15]. Guérin, D. M., Lascombe, M. B., Costabel, M., Souchon, H., Lamzin, V., Béguin, P., & Alzari, P. M.

(2002). Atomic (0.94 Å) resolution structure of an inverting glycosidase in complex with substrate. *Journal of molecular biology*, 316(5), 1061-1069.

[16]. Bhardwaj, A., Mahanta, P., Ramakumar, S., Ghosh, A., Leelavathi, S., & Reddy, V. S. (2012). Emerging role OF N-and C-terminal interactions IN stabilizing ( $\beta;/\alpha$ ) 8-fold with special emphasis ON family 10 xylanases. *Computational and Structural Biotechnology Journal*, 2(3), e201209014.